Exploring Vehicular Interaction from Trajectories Based on Granger Causality

Xishun Liao*, Guoyuan Wu*, Matthew J. Barth*, Rohit Gupta†, and Kyungtae Han†

2023 IEEE Intelligent Vehicles Symposium (IV) | 979-8-3503-4691-6/23/$31.00 ©2023 IEEE | DOI: 10.1109/IV55152.2023.10186803

***Abstract*—Understanding the behavior of human drivers and how they interact with other drivers is crucial to develop and improve the decision-making capabilities of connected and automated vehicles (CAVs). This allows CAVs to anticipate and proactively respond to the actions of other road users in a safe and efficient manner, especially in mixed-traffic environments. Most existing studies rely on neural networks to model such interaction implicitly, and very few studies attempt to interpret the interaction. Considering its interpretability and flexibility, the Granger causality (GC) framework is widely used to understand the relationships between different agents, as well as how these relationships change over time. In this paper, we integrate the knowledge of traffic and vehicle dynamics into the neural network to learn the Granger causality and explore vehicular interaction from multi-vehicle trajectories. The proposed algorithm has been validated using both the INTERACTION dataset and field data collected in Riverside, California. The results show that our algorithm is able to address three key questions regarding vehicular interaction: 1) whether the interactions exist between/among the vehicles; 2) when the interactions occur and terminate; and 3) how strong the interactions between/among vehicles are.**

***Index Terms*—Vehicular interaction, Granger causality, Personalized behavior, Multi-agent system**

I. Introduction

A. Motivation

In the foreseeable future, connected and automated vehicles (CAVs) need to share the road and interact with other human-driven vehicles in a mixed traffic environment, where a CAV actively observes its surrounding vehicles' states, predicts other vehicles' behaviors, makes decisions and executes the action. Discovering the interaction pattern among vehicles from the observed data can improve the prediction and decision-making process, enabling CAV to better coordinate with its surroundings in a safer and more efficient manner.

The increasing amount of vehicle trajectory data has led to data-driven methods for automatically learning the interaction. Most existing studies encode and learn the interaction among agents implicitly as a middle layer of neural networks [1]–[3], which undermines the interpretability and transferability of the learned interaction model. In this study, we aim to model interaction explicitly and address the questions of *who* is involved in the interaction, *when* does the interaction occur, and *how* to quantify it, with an interpretable data-driven model. To identify the complex and implicit vehicle interaction, this study relies on the definition proposed by Markkula et al. [4], who indicate that in an interaction, two or more vehicles should be involved, should be influenced by each other, and should have spatiotemporal conflicts with other vehicles.

Due to its interpretability, Granger causality (GC) [5] is a practical method to analyze interactions on a set of time series, especially for systems with nonlinear dynamics. Recently, it is widely adopted in many fields, including neuroscience, social media analysis, climate science, and econometrics [6], [7]. Similarly, exploring the interaction among vehicles based on the trajectory can be considered a problem of multivariate time series analysis. Therefore, in this paper, a GC-based approach is used to explore the interactions among a multi-vehicles system.

B. Literature Review

1) Data-driven vehicular interaction modeling: Many vehicle interaction studies have been applied to extracting interaction patterns from observed vehicle trajectories. Considering limited computational resources in real-time, Refaat et al. [8] prioritized surrounding agents for the planning process, based on their influence on the ego vehicle. Also, the attention mechanism is a popular interaction encoding method as it can evaluate the similarity or importance between vectorized series [9]. To quantify the influence of others on ego vehicle, Leurent and Mercat [10] calculated the attention value between ego vehicle and its surrounding agents and hence improved the prediction result. In addition to analyzing such influence, interaction study considers the mutual effect. Researchers [11]–[13] modeled the vehicle interaction using graph neural network (GNN), which can capture the correlation between nodes (i.e., vehicles) and encode the interaction intensity in the learnable weights of graph edges. To capture both the influence and interaction, graph attention networks (GAT) were adopted to update the vehicle features by considering the influence from other nodes [14]. However, supervised or semi-supervised methods are limited by data labeling cost, and GNN is not flexible in dynamic environments because the graph cannot handle large variations in the number of nodes (i.e., agents) [15]. Other researchers explored parametric methods such as social value orientation (SVO) [16], [17] and inverse reinforcement learning (IRL) [18], [19] for understanding drivers' interaction preference. Although these models are explainable, they learn fixed parameters by using historical data and cannot update in real time. Moreover, the aforementioned methods cannot explicitly explain the interaction by addressing three key questions related to '*who*', '*when*', and '*how*'.

Corresponding author: Xishun Liao, xliao016@ucr.edu

*Department of Electrical and Computer Engineering, and the Center for Environmental Research and Technology, University of California, Riverside, CA 92507.

†InfoTech Labs, Toyota Motor North America R&D, Mountain View, CA 94043.

2) Granger causality: Granger causality was developed in 1969 by Granger [5] and now became one of the most popular approaches for temporal causal discovery. This paper adopted its general form for non-linear systems, and many existing methods can be adapted into this form, such as vector autoregression (VAR) [20] and deep learning methods [21], [22].

Consider observing trajectories from *N* vehicles, and each trajectory contains P features f across time span $t = \{1, \ldots, T\}$, i.e., $X = \left\{x^1_{<t}, \ldots, x^N_{<t}\right\}, x^i_t = \{f_1, \ldots, f_P\}$. A non-linear function g^i (e.g., nonlinear VAR) is used to capture how the past of all N vehicles influences the i^{th} vehicle, such that

$$x^i_{t+1} = g_i\left(x^1_{<t}, \ldots, x^N_{<t}\right) + e^i_t \tag{1}$$

where e^i_t is noise term. If g^i is independent on other vehicle $x^j_{<t}$, vehicle $x^j_{<t}$ is irrelevant in the prediction of vehicle x^i. Then, the above can be concluded that [7] time series x^j is noncausal for time series x^i, if and only if for all $\left\{x^1_{<t}, \ldots, x^N_{<t}\right\}$ and all $x^{j\prime}_{<t} \neq x^j_{<t}$, such that

$$g^i\left(x^1_{<t}, \ldots, x^j_{<t}, \ldots, x^N_{<t}\right) = g^i\left(x^1_{<t}, \ldots, x^{j\prime}_{<t}, \ldots x^p_{<t}\right) \tag{2}$$

However, false causality may be discovered by only relying on data-driven GC. To improve the reliability of the model, expert knowledge of the study field needs to be integrated into the model. Moreover, instead of defining the system mechanism [23], GC is usually used to investigate complex systems that are difficult to be modeled and to provide a system-level perspective of the interaction.

C. Contribution

In this paper, we claim the following key contributions:

- We propose an unsupervised data-driven approach to model the multi-vehicle interaction, as one of the first research that implements Granger causality on a vehicular motion study;
- Regularized by social norms and road geometry, the proposed explainable network is able to quantify the interaction and can be validated in a reliable manner; and
- Besides the demonstration on the INTERACTION dataset, the proposed algorithm is implemented on a personalized dataset and discovers personalized interaction patterns for two drivers.

II. Methodology

In this study, we propose a framework to evaluate the multi-vehicle interaction, which consists of a vehicle behavior model based on potential field theory and a GC discovery process. Similar to the vehicle interaction, movement ecology also considers complicated perception, planning, and execution process. By integrating a conceptual ecology behavioral model [24], Fujii et al. [22] proposed a GC-based inference framework to study the multi-animal interaction, and the performance for GC discovery was validated in the labeled synthetic dataset (e.g., nonlinear oscillator and boid model simulation) and real-world animal dataset. But vehicle movement is more constrained by the social norms (safe behavior) of human drivers and road geometry. To include scientific knowledge regularization, we apply potential field theory in Frenet coordinate [25] to encode the social norms. Overall, as shown in Fig. 1, the system inputs are the trajectories of all analyzed vehicles, and the two outputs are the coefficient matrices of GC values for interaction intensity evaluation and prediction results of each vehicle provided by generalized vector autoregression (GVAR). Finally, the interaction intensity is quantified by the strength of GC effect in the coefficient matrix, as they explain how the past of other vehicles contributes to the future of the evaluated vehicle.

A. GC Discovery using GVAR under SENN Structure

1) Self-explaining neural networks (SENN): A SENN [26] represents a class of intrinsically interpretable models, and it consists of a link function $G(\cdot)$ and interpretable basis $h(x)$, following the form:

$$f(\boldsymbol{x}) = G\left(\theta(\boldsymbol{x})_1 h(\boldsymbol{x})_1, \ldots, \theta(\boldsymbol{x})_k h(\boldsymbol{x})_k\right) \tag{3}$$

where x are predictors, $\theta(\cdot)$ is a neural network with k outputs. $\theta(x)$ is the coefficient for x and is used to explain the contribution of each basis to prediction result $f(x)$. After simplification, Equation (3) can be written as:

$$f(\boldsymbol{x}) = \sum_{j=1}^{p} \theta(\boldsymbol{x})_j x_j \tag{4}$$

2) Generalized vector autoregression: In a vehicle interaction study, the trajectory of each involved vehicle is considered as a basis to predict the target vehicle, and the contribution of each basis 'explains' the influence of each vehicle, which is indicated by $\theta(x)$. SENN was applied to infer GC in a multivariate system by Marcinkevics and Vogt [20], who extended VAR to generalized vector autoregression (GVAR) as the link function, and the GVAR is expressed as

$$\mathbf{x}_t = \sum_{k=1}^{K} \boldsymbol{\Phi}_{\boldsymbol{\theta}_k}\left(\mathbf{x}_{t-k}\right) \mathbf{x}_{t-k} + \varepsilon_t \tag{5}$$

where the $\boldsymbol{\Phi}_{\boldsymbol{\theta}_k}$ is a neural network parameterized by θ_k. Then $\boldsymbol{\Phi}^i_{t,k} = \boldsymbol{\Phi}_{\boldsymbol{\theta}_k}\left(\mathbf{x}_{t-k}\right)$ is a coefficient matrix for lag k and time t, and the element (i, j) of $\boldsymbol{\Phi}^i_{t,k}$ is the influence of time step $\mathbf{x}^j_{t-k}$ on $\mathbf{x}^i_t$.

The dash-box in Fig. 1 illustrates the calculation for the coefficient matrix $\boldsymbol{\Phi}^i_t$ and prediction result using Equation (5) with an order-K GVAR. The matrix $\boldsymbol{\Phi}^i_t$ captures the influence of other vehicle on vehicle i at time t, with f_R, f_N, and f_M representing the regulation, navigation, and movement functions, respectively. These functions are introduced in the following subsections. To obtain the whole coefficient matrix for the whole group, the generalized coefficient matrix of N vehicles are concatenated at each time step.

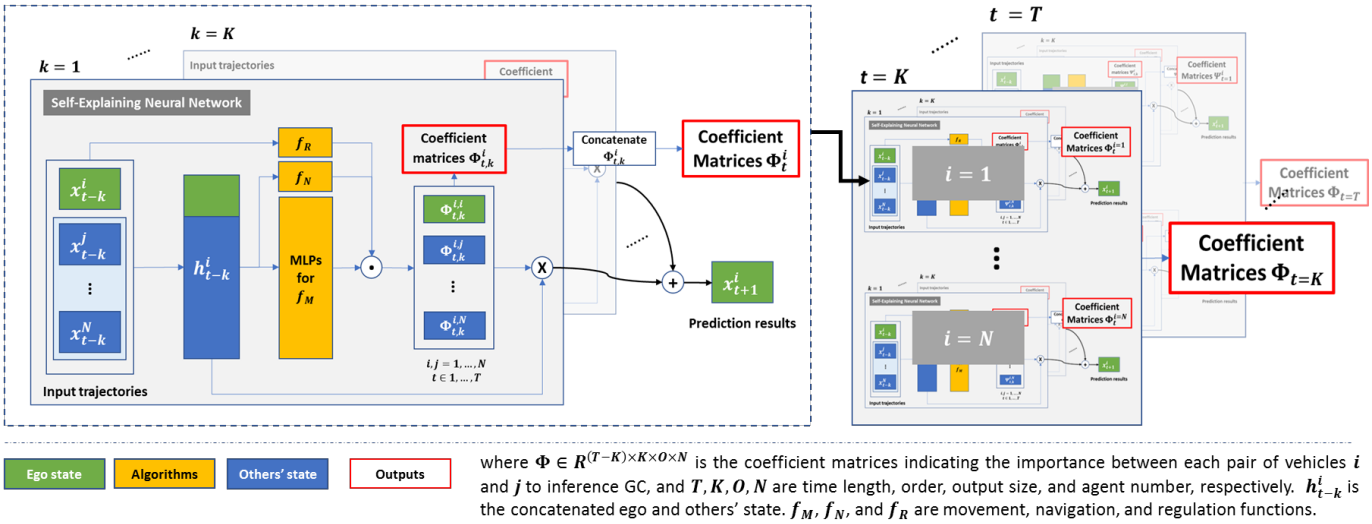

Fig. 1. Generalized vector autoregression under self-explaining neural network structure for Granger causality discovery.

Therefore, the strength of the influence (i.e., GC effect [22]) between time series x^i and x^j can be explored by inspecting the generalized coefficient matrix $\mathbf{\Phi}_t = \mathbf{\Phi}_{\boldsymbol{\theta}_k}(x_t)$, as Equation (6):

$$GC^{i,j} = \underset{\substack{1\le k\le K\\ K+1\le t\le T}}{\text{signmax}} \left\{ \underset{\substack{1\le k\le K\\ K+1\le t\le T}}{\text{median}} \left(\mathbf{\Phi}_{\boldsymbol{\theta}_k}(\boldsymbol{x}_t)\right)_{i,j} \right\} \cdot \underset{1\le k\le K}{max} \left\{ \underset{K+1\le t\le T}{median} \left(\left| \left(\mathbf{\Phi}_{\boldsymbol{\theta}_k}(\boldsymbol{x}_t)\right)_{i,j} \right| \right) \right\} \quad (6)$$

where $signmax$ function outputs the sign of the number that has the largest absolute value.

B. Vehicle Movement Model

To avoid problematic results (e.g., linking vehicles that are too far apart) for vehicle interaction, the aforementioned knowledge (i.e., social norms) needs to be incorporated into the SENN-GVAR model. Instead of relying on one neural network $\mathbf{\Phi}_{\boldsymbol{\theta}_k}$ in Equation (5), we decompose the vehicle movement model into three processes to make the movement model interpretable and reliable, including social norm regularization, navigation, and planning processes (i.e., f_R, f_N, f_M, respectively, as the yellow blocks in Fig. 1 shows). Thus, the $\mathbf{\Phi}_{\boldsymbol{\theta}_k}$ in Equation (5) is extended to Equation (7). This subsection discusses how each process in the vehicle movement model is formulated and integrated into the GVAR model.

$$\mathbf{\Phi}_{\boldsymbol{\theta}_k}(\mathbf{x}_{t-k}) = f_{R_k}(\boldsymbol{x}_{t-k}) \odot f_{N_k}(\boldsymbol{x}_{t-k}) \odot f_{M_k}(\boldsymbol{x}_{t-k}) \quad (7)$$

$$\begin{cases} E_v = M_i \rho \frac{e^{-\beta_1 a \cos\theta_0}}{|k'|} \cdot \frac{k'}{|k'|} \\ M_i = m_i \left(1.566 \times 10^{-14} v^{6.687} + 0.3345\right) \\ |k'| = \sqrt{\left[(x^* - x_0)\frac{\tau}{e^{\alpha v}}\right]^2 + \left[(y^* - y_0)\tau\right]^2} \\ \begin{bmatrix} x^* \\ y^* \end{bmatrix} = \begin{bmatrix} \cos\phi & \sin\phi \\ -\sin\phi & \cos\phi \end{bmatrix} \begin{bmatrix} x \\ y \end{bmatrix} \end{cases} \quad (8)$$

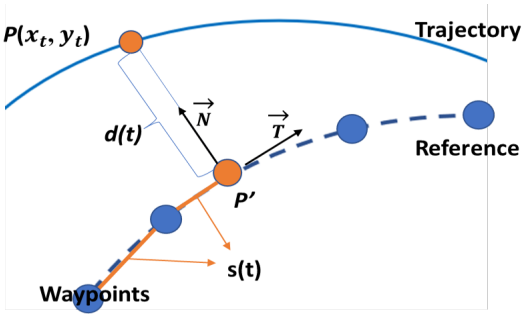

Fig. 2. Mapping object in Cartesian coordinate to Frenet coordinate.

1) Regularization process: The social regularization f_R is formulated to estimate the conflict level with surrounding vehicles based on the region of interest (RoI) of the analyzed vehicle. Driving safety is a critical factor in interaction studies, and drivers are assumed to pay more attention to the conflicting vehicles that may pose a threat. Since the risk cannot be simply evaluated by Euclidean distance, the potential field becomes a powerful tool for social norm encoding [15] and understanding how drivers perceive their surroundings. To characterize the driving risk level for ego vehicle, Li et al. [27] proposed a potential field equation for vehicle control, whose parameters were calibrated with real-world data, as shown in Equation (8). In this paper, the value of risk level is adapted to estimate the RoI of the analyzed vehicle, by proportionally expanding the field based on the 3-second rules [28]. Besides the social norm, road geometry needs to be included. Therefore, we calculate the RoI in Frenet coordinate, instead of Cartesian coordinate. As shown in Fig. 2, vehicle state (e.g., longitudinal position $s(t)$ and lateral position $d(t)$) in Frenet coordinate is calculated based on the reference lane (e.g., the center line of the lane). At each time step, *Algorithm 1* generates an RoI for each vehicle as shown in Fig. 3, where the red dot stands for the analyzed vehicle, and blue dash

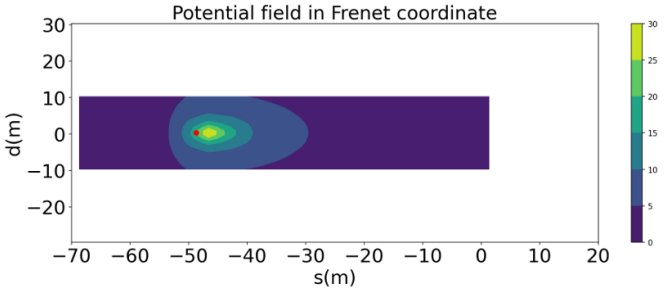

(a) RoI of the analyzed car in Frenet frame

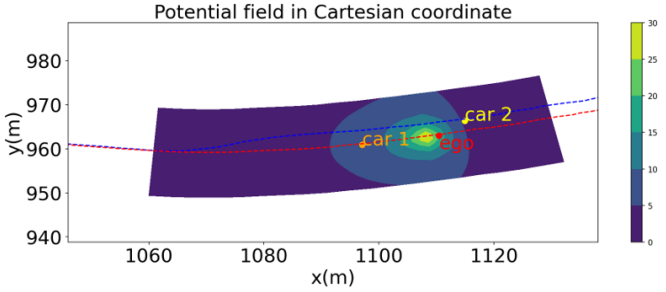

(b) Conflict level of other vehicles within RoI

Fig. 3. An example of estimating the conflict level of surroundings based on potential field theory.

***Algorithm 1*: Conflict Level Estimation using Potential Field**

Input: (1) The reference lane. (2) State of all vehicles.

Output: The conflicting levels $\boldsymbol{f_R^{j\to i}}$ of others to analyzed vehicle

1: Convert Cartesian (x_t, y_t) to Frenet frame (s_t, d_t) for the vehicle state of the analyzed vehicle

2: Create a grid map $G(s,d)$ centered on (s_t, d_t)

3: Calculate risk value $E(s,d)$ for the grid based on Equation (8)

4: Find the contour S_c of 95th-percentile (2σ) of $E(s,d)$

5: Calculate ratio $r = 3 \cdot v/max(S_c)$, where $3 \cdot v$ follows the three-second rule

6: Expand the grid map $G'(s',d') = G(s,d) \cdot r$, and obtain the $E(s',d')$

7: Convert $E(s',d')$ in Frenet frame to $\boldsymbol{E(x,y)}$ Cartesian frame

8: Calculate the risk level $\boldsymbol{R^{j\to i}}$ of other vehicle V^j, based on the position $P^j(x,y)$ on $\boldsymbol{E(x,y)}$

9. $\boldsymbol{f_R^{j\to i} = R^{j\to i}/max(E(x,y))}$.

Return: $\boldsymbol{f_R^{j\to i}}, \forall j = 1, \ldots, N, j \neq i$

lines and red dash lines are the reference lanes. Based on the RoI, the conflict level of other vehicles can be estimated by considering road geometry and the analyzed vehicle state.

2) Navigation and movement process: The navigation process f_N is a sign function to capture the car-following behavior between ego vehicle i and vehicle j , and $f_N\left(\boldsymbol{x}^{i,j}\right) = 2\sigma\left(\Delta\boldsymbol{v}^{i,j}/w_n\right) - 1$, where σ is a sigmoid function, $\Delta\boldsymbol{v}^{i,j}$ is the speed difference, and w_n is a learnable coefficient. $f_N > 0$ indicates attraction, i.e., the vehicle tries to close the car-following gap, and $f_N < 0$ means repulsion, i.e., the opening gap behavior. The movement process f_M^i is constructed by two-layer MLPs for each order and vehicle.

The loss function for training the whole GVAR consists of mean square prediction error (MSE), sparsity-inducing penalty [29] (i.e., $\mathcal{L}_s = \alpha \left\|\Phi_t\right\|_1 + (1-\alpha)\left\|\Phi_t\right\|_F^2$), and a theory-guided regularization term $\mathcal{L}_{TG}$ from [22]. $\mathcal{L}_{TG}$ is adopted with the assumption that the vehicle goes straight following the center line from the current state if no interaction is detected, as shown in Equation (9). The whole loss function can be written by Equation (10).

$$\mathcal{L}_{TG}\left(\boldsymbol{\Phi}_t\right) = \exp\left(\left\|\boldsymbol{x}_t - \tilde{\boldsymbol{x}}_t\right\|_2^2/\eta\right)\left\|\boldsymbol{\Phi}_t'\right\|_t^2 \tag{9}$$

where the $\tilde{\boldsymbol{x}}_t$ is the intuitive prediction (i.e., assuming vehicle stays on the center line with a deviation constrained by a threshold η.), $\boldsymbol{\Phi}_t'$ is the coefficient matrix regarding others by excluding the weights for ego vehicle from $\boldsymbol{\Phi}_t$.

$$\mathcal{L} = \frac{1}{T-K}\sum_{t=K+1}^{T}\left(\left\|\boldsymbol{x}_t - \hat{\boldsymbol{x}}_t\right\|_2^2 + \lambda\mathcal{L}_s + \gamma\mathcal{L}_{TG}\right) \tag{10}$$

C. Permutation Feature Importance for Causality Validation

The cause discovered by GC is the potential cause, which needs to be validated. Besides the visualization of GC value (presented in Section III), we use permutation feature importance (PFI) [30] to validate the proposed data-driven method without ground truth for interaction. PFI measures a method for determining the importance of a feature in a machine learning model, and similarly, it is used to understand the contribution of a vehicle to the overall prediction. It works by randomly shuffling the values of the trajectory of the target vehicle, and measuring the change in the model's performance.

On the other hand, PFI is a powerful technique to validate the result of GC. Since causality discovery relies on temporal information, the permutation process can remove chronological information and causal relation between the target vehicle and the rest of the system, before re-sending the data into the GC-based network. Also, PFI introduces no confounding factor to affect the prediction, as permutation does not change the distribution of the dataset. The validation process based on PFI is described in *Algorithm 2*.

III. Case Study and Result Analysis

In order to validate the proposed GC-based vehicle interaction modeling approach, we studied the vehicle interaction in a real-world on-ramp merging scenario, which requires the coordination of lateral and longitudinal control from drivers, making it a highly interactive and conflicting scenario. In this section, the proposed algorithm reveals how the studied vehicle influences others and is influenced in a four-vehicle merging scenario. Moreover, the algorithm recognizes the personalized interaction patterns of two drivers with different driving styles, using their historical datasets.

A. Vehicular interaction interpretation Using INTERACTION dataset

Among various datasets, we demonstrate the proposed algorithm on the INTERACTION dataset [31], which provides HD maps and motions of all vehicles which may influence driving behavior. Trajectories of each vehicle include the timestamp, position (x, y), speed (v_x, v_y), and heading angle. The selected ramp merging scenario is presented in Fig. 4, where the center

***Algorithm 2*: Vehicle Contribution Analysis based on PFI**

Input: (1) Trained network model. (2) Input dataset $\boldsymbol{X}$.
Output: An importance matrix $\boldsymbol{M_{PFI}}$ for $\boldsymbol{N}$ vehicles

```
Create M_PFI ∈ R^N
Run the trained network on dataset X
Measure the loss L_o
for each vehicle x^i in system:
    Create X_perm by permuting features of vehicle x^i
    Run the trained network on the X_perm
    Measure the intervention prediction loss L_p^i of x^i
    Calculate importance as quotient FI^i = L_p^i / L_o
    M_PFI(i) = FI^i
```

Return: $\boldsymbol{M_{PFI}}$

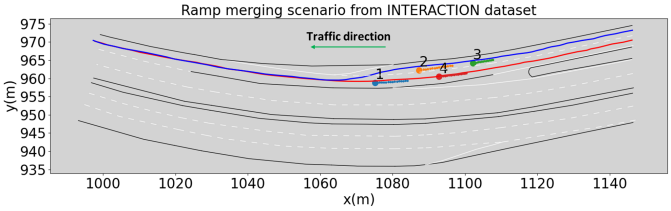

Fig. 4. On-ramp merging scenario from INTERACTION dataset.

lines of the ramp and mainline are extracted from the HD map, and a four-vehicle group is chosen as the study case.

Once Φ'_{θ_k} in Equation (7) is trained, the vehicular interaction intensity ($GC^{i,j}$) can be assessed by Equation (6). The four-vehicle interaction during the merging process is elaborated in Fig. 5. Fig. 5(a) presents four key events during the merging, where the blue and red dash lines are the ramp and mainline, respectively. Vehicles are numbered based on their appearance order with tails of past 1.5 seconds (15-time steps), and a longer tail implies higher speed. The $GC^{i,j}$ throughout time is described in 5(b), e.g., (i, j) graph is the influence of vehicle #i on vehicle #j. A positive value means attraction and following, while a negative value stands for repulsion and implies that rather than reacting to another's action, the agent tends to take the lead. Moreover, in each graph, four vertical dash lines mark the four key events in 5(a) correspondingly.

The blue solid line in 5(b) shows that the proposed algorithm can detect the most interactive at each time step for each vehicle. At t=24, vehicle #4 joins the group with a higher speed (longer tail). According to graph (4,1) in 5(b), #4 is significantly affected by #1 since it has to slow down and follows #1. Also, #4 competes for the merging priority with #3 and tries to lead #3, and this movement is reflected on both graph (4,3) and (3,4). At the same time, #2 is taking the lead over #4 and shows a strong will to compete. At t=108, since #1 speeds up and leaves everyone behind, its influence on others decreases, and others have little influence on #1. At the moment, #2 takes #4 as the most important competitor and accelerates, while most of #4's attention is on #3. When t=171, the competition of merging order is settled, so the interaction intensity among vehicles becomes more stable, except for #2,

TABLE I
PERMUTATION FEATURE IMPORTANCE (PFI) ANALYSIS

Vehicles	#1	#2	#3	#4
Influence Level*	312.18	327.81	390.99	434.45
Final Epoch Loss	1.39			
Permutation Loss	1.02	1.27	1.73	2.04
$Quotion - PFI$	0.66	0.91	1.25	1.46

$*$ A vehicle's overall influence level is measured by the sum of its GC value over time and GC values of other agents, i.e., the influence level of x^i is $\sum_{j\in N, j\neq i}^{N}\sum_{t}^{T}\left|GC^{ij}\right|$

which starts merging into the mainline and needs to maintain a safe car-following gap to #1. At t=221, the last vehicle #3 finishes its merging. The answer to *who* involves in interaction and *when* the interaction happens can be solved by setting an intensity threshold, based on algorithms that distinguish the difference between non-interactive state and interactive state.

As the baseline, GVAR has no information about the road constraint and social norms in traffic and generates counter-intuitive results, as the orange dash line in Fig.5(b) shows. For example, GVAR misjudges that the far upstream vehicles affect #1, as in graph (1,3) (1,4) (2,3). In addition, although #3 increases the car-following gap to #2 and switches to follow #4 at t=108, the effect of #2 on #3 is maintained till the end by GVAR, as in graph (3,2). Moreover, GVAR ignores the perception limitation of #3 and identifies an increasing effect of #1 on #3 at the end of the graph (3,1), even though there are two vehicles in between.

The contribution of each vehicle to the system prediction is indicated by its PFI value, as listed in Table I. A vehicle's PFI value aligns with its GC value. In other words, if the influence (measured by its GC) level is higher over time, its PFI is higher. For instance, #1 contributes the least, so both values of its GC and PFI are low. On the other hand, the PFI values of #4 are the highest since it interacts with both #2 and #3. It should be noted that a vehicle's GC value does not include its contribution to its own prediction, therefore, there is no linear mapping relationship between GC and PFI.

B. Personalized interaction pattern discovery

Understanding how individuals interact with other vehicles and the interactions differ from each other allows engineers to design personalized vehicles that better meet the needs and preferences of different drivers. To study the personalized interaction behavior, we implement the proposed algorithm on a personalized dataset of two drivers from our previous study [32]. The dataset was collected in ramp merging field experiments that are carried out at an on/off-ramp section along Columbia Ave., Riverside, CA. The experiment created merge interactions between a ramp vehicle and a mainline vehicle and collected 20 merging trips for each studied ramp driver and an anonymous mainline driver. In the driver behavior analysis, Driver 1 was found to be more conservative and usually merged behind the mainline vehicle. In contrast, Driver 2 was more aggressive and always accelerated to merge in front of the mainline vehicle.

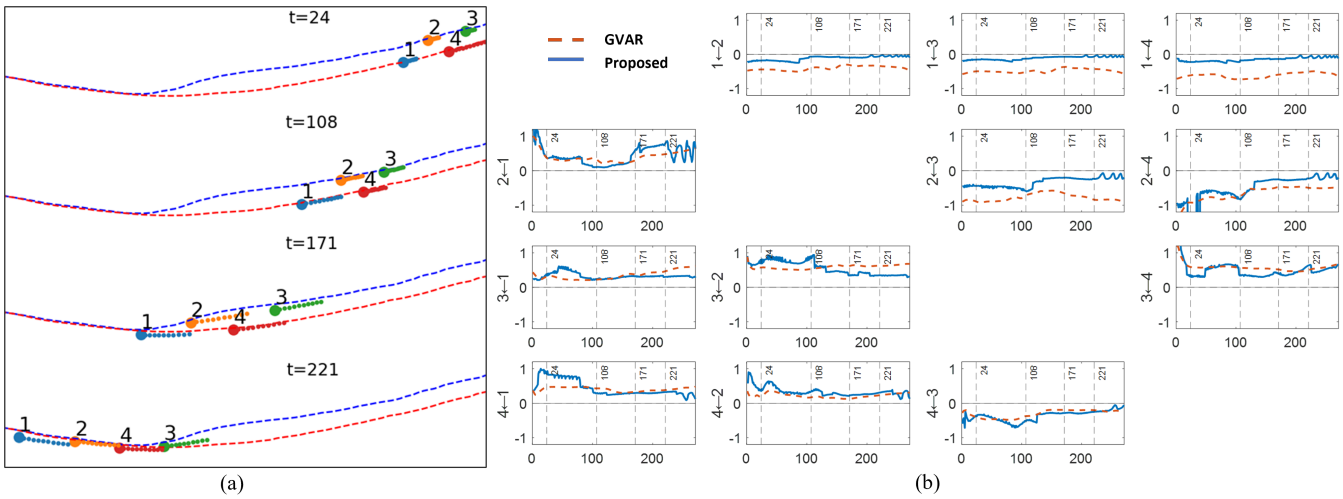

(a) (b)

Fig. 5. Interaction process during a four-vehicle merging. (a) Key moments during the merging process. (b) Interaction intensity among vehicles.

Fig. 6 illustrates the personalized interaction pattern during ramp merging trips for these two drivers. The red line is the average interaction intensity for the studied ramp driver, and the blue line is for the conflicting mainline driver. For conservative Driver 1 in 6(a), the interaction between two drivers is mild, with a maximum intensity value of 0.41. The positive intensity value of Driver 1 shows an attraction to the mainline vehicle, which leads the movement of Driver 1. Compared to Driver 1, Driver 2 involves stronger interactions in 6(b), where the maximum absolute intensity is 0.92, and the intensity variance is much larger than Driver 1's. For most of the time, the interaction intensity of Driver 2 is negative, since Driver 2 prefers to take the lead and merge in front.

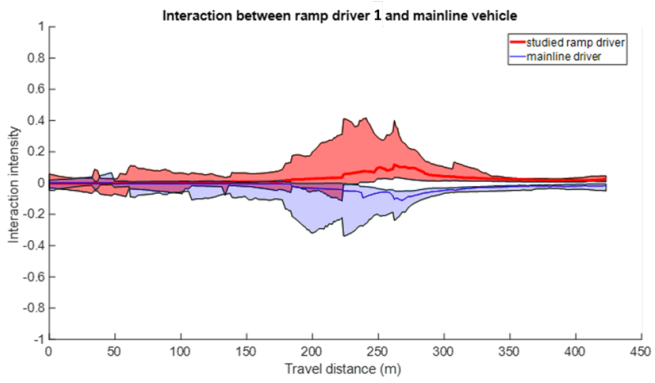

(a) Aggregated interaction pattern of conservative ramp car driver 1

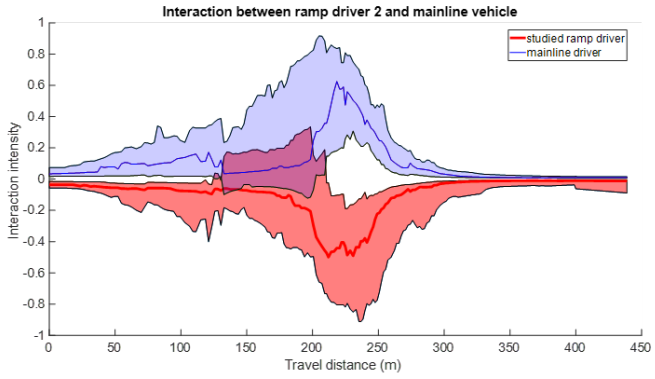

(b) Aggregated interaction pattern of aggressive ramp car driver 2

Fig. 6. Personalized interaction pattern analysis in ramp merging scenario.

IV. Discussion

Implications. The goal of this study is to provide an interpretable data-driven method to discover the interaction pattern from observed vehicle trajectories. As a result, the mutual influences among vehicles are quantified by the strength of the GC effect, and we are able to answer the unsettled questions of *who*, *when*, and *how* for interaction study. The proposed method in this paper lays a solid foundation for a suite of downstream applications, including multi-vehicle trajectory prediction, traffic organization, and motion planning. For example, this method can be used as an automatic data labeling tool to encode interaction information into the neural networks for prediction purposes. Also, if the interaction intensity is too high, traffic control (e.g., ramp metering) can be implemented to relieve the competition among vehicles considering safety. Finally, personalized interaction can be studied for specific drivers by following this protocol. Knowing the personalized interaction preference can help customize the vehicle setup for a personalized advanced driver assistance system, enabling the vehicle to interact with others in dynamic environments. Moreover, modeling personalized interaction contributes to driving style recognition and personality inference [33].

Limitations. One obvious shortcoming of using GC is that the VAR-based prediction methods cannot capture long-term temporal dependency whenever GC takes the advantage of VAR's simple structure. Similar to other unsupervised methods, validating the interaction without ground truth is still challenging. Toward this end, Granger causality is not the real cause, and the result may not be the only cause. However, it can be used as an analytical tool to reveal the interaction within a system.

V. Conclusions

In this paper, we quantify the multi-vehicle interaction using an explainable data-driven approach, which is one of the first implementations of Granger causality on vehicle motion study. To improve accuracy and interpretability, the proposed approach integrates social norms and road geometry into the network. An on-ramp merging scenario with real-world data is used to demonstrate the algorithm performance, and permutation feature importance is used to validate the result for this unsupervised algorithm. Finally, the algorithm is implemented on a personalized driving dataset for personalized interaction pattern recognition.

As the first few GC implementations in the vehicle movement domain, there are many future directions worth exploring. For example, the interaction between vehicles and infrastructure (e.g., traffic lights and traffic signs) can be considered since the movement of vehicles is also influenced by static objects on road. We will use the proposed method as a data labeling tool for network training to enable interaction-aware prediction. Discovering personalized interaction patterns for P-ADAS development can be also one of our future studies.

References

[1] M. Liang, B. Yang, R. Hu, Y. Chen, R. Liao, S. Feng, and R. Urtasun, "Learning lane graph representations for motion forecasting," in *European Conference on Computer Vision*. Springer, 2020, pp. 541–556.

[2] Y. Yuan, X. Weng, Y. Ou, and K. M. Kitani, "Agentformer: Agent-aware transformers for socio-temporal multi-agent forecasting," in *Proceedings of the IEEE/CVF International Conference on Computer Vision*, 2021, pp. 9813–9823.

[3] J. Ngiam, B. Caine, V. Vasudevan, Z. Zhang, H.-T. L. Chiang, J. Ling, R. Roelofs, A. Bewley, C. Liu, A. Venugopal *et al.*, "Scene transformer: A unified architecture for predicting multiple agent trajectories," *arXiv preprint arXiv:2106.08417*, 2021.

[4] G. Markkula, R. Madigan, D. Nathanael, E. Portouli, Y. M. Lee, A. Dietrich, J. Billington, A. Schieben, and N. Merat, "Defining interactions: A conceptual framework for understanding interactive behaviour in human and automated road traffic," *Theoretical Issues in Ergonomics Science*, vol. 21, no. 6, pp. 728–752, 2020.

[5] C. W. Granger, "Investigating causal relations by econometric models and cross-spectral methods," *Econometrica: journal of the Econometric Society*, pp. 424–438, 1969.

[6] J. M. McCracken, "Exploratory causal analysis with time series data," *Synthesis Lectures on Data Mining and Knowledge Discovery*, vol. 8, no. 1, pp. 1–147, 2016.

[7] A. Shojaie and E. B. Fox, "Granger causality: A review and recent advances," *Annual Review of Statistics and Its Application*, vol. 9, pp. 289–319, 2022.

[8] K. S. Refaat, K. Ding, N. Ponomareva, and S. Ross, "Agent prioritization for autonomous navigation," in *2019 IEEE/RSJ International Conference on Intelligent Robots and Systems (IROS)*. IEEE, 2019, pp. 2060–2067.

[9] A. Vaswani, N. Shazeer, N. Parmar, J. Uszkoreit, L. Jones, A. N. Gomez, Ł. Kaiser, and I. Polosukhin, "Attention is all you need," *Advances in neural information processing systems*, vol. 30, 2017.

[10] E. Leurent and J. Mercat, "Social attention for autonomous decision-making in dense traffic," *arXiv preprint arXiv:1911.12250*, 2019.

[11] D. Cao, J. Li, H. Ma, and M. Tomizuka, "Spectral temporal graph neural network for trajectory prediction," in *2021 IEEE International Conference on Robotics and Automation (ICRA)*. IEEE, 2021, pp. 1839–1845.

[12] A. Mohamed, K. Qian, M. Elhoseiny, and C. Claudel, "Social-stgcnn: A social spatio-temporal graph convolutional neural network for human trajectory prediction," in *Proceedings of the IEEE/CVF Conference on Computer Vision and Pattern Recognition*, 2020, pp. 14 424–14 432.

[13] O. Makansi, J. Von Kügelgen, F. Locatello, P. Gehler, D. Janzing, T. Brox, and B. Schölkopf, "You mostly walk alone: Analyzing feature attribution in trajectory prediction," *arXiv preprint arXiv:2110.05304*, 2021.

[14] V. Kosaraju, A. Sadeghian, R. Martín-Martín, I. Reid, H. Rezatofighi, and S. Savarese, "Social-bigat: Multimodal trajectory forecasting using bicycle-gan and graph attention networks," *Advances in Neural Information Processing Systems*, vol. 32, 2019.

[15] W. Wang, L. Wang, C. Zhang, C. Liu, L. Sun *et al.*, "Social interactions for autonomous driving: A review and perspectives," *Foundations and Trends® in Robotics*, vol. 10, no. 3-4, pp. 198–376, 2022.

[16] W. Schwarting, A. Pierson, J. Alonso-Mora, S. Karaman, and D. Rus, "Social behavior for autonomous vehicles," *Proceedings of the National Academy of Sciences*, vol. 116, no. 50, pp. 24 972–24 978, 2019.

[17] N. Buckman, A. Pierson, W. Schwarting, S. Karaman, and D. Rus, "Sharing is caring: Socially-compliant autonomous intersection negotiation," in *2019 IEEE/RSJ International Conference on Intelligent Robots and Systems (IROS)*. IEEE, 2019, pp. 6136–6143.

[18] Z. Zhao, Z. Wang, K. Han, R. Gupta, P. Tiwari, G. Wu, and M. J. Barth, "Personalized car following for autonomous driving with inverse reinforcement learning," in *2022 International Conference on Robotics and Automation (ICRA)*, 2022, pp. 2891–2897.

[19] X. Liao, Z. Wang, X. Zhao, Z. Zhao, K. Han, P. Tiwari, M. Barth, and G. Wu, "Online prediction of lane change with a hierarchical learning-based approach," in *Proceedings 2022 IEEE International Conference on Robotics and Automation. IEEE*, 2022.

[20] R. Marcinkevičs and J. E. Vogt, "Interpretable models for granger causality using self-explaining neural networks," *arXiv preprint arXiv:2101.07600*, 2021.

[21] A. Tank, I. Covert, N. Foti, A. Shojaie, and E. Fox, "Neural granger causality for nonlinear time series," *stat*, vol. 1050, p. 16, 2018.

[22] K. Fujii, N. Takeishi, K. Tsutsui, E. Fujioka, N. Nishiumi, R. Tanaka, M. Fukushiro, K. Ide, H. Kohno, K. Yoda *et al.*, "Learning interaction rules from multi-animal trajectories via augmented behavioral models," *Advances in Neural Information Processing Systems*, vol. 34, pp. 11 108–11 122, 2021.

[23] A. B. Barrett and L. Barnett, "Granger causality is designed to measure effect, not mechanism," *Frontiers in neuroinformatics*, vol. 7, p. 6, 2013.

[24] R. Nathan, W. M. Getz, E. Revilla, M. Holyoak, R. Kadmon, D. Saltz, and P. E. Smouse, "A movement ecology paradigm for unifying organismal movement research," *Proceedings of the National Academy of Sciences*, vol. 105, no. 49, pp. 19 052–19 059, 2008.

[25] M. Werling, J. Ziegler, S. Kammel, and S. Thrun, "Optimal trajectory generation for dynamic street scenarios in a frenet frame," in *2010 IEEE International Conference on Robotics and Automation*. IEEE, 2010, pp. 987–993.

[26] D. Alvarez Melis and T. Jaakkola, "Towards robust interpretability with self-explaining neural networks," *Advances in neural information processing systems*, vol. 31, 2018.

[27] L. Li, J. Gan, K. Zhou, X. Qu, and B. Ran, "A novel lane-changing model of connected and automated vehicles: Using the safety potential field theory," *Physica A: Statistical Mechanics and its Applications*, vol. 559, p. 125039, 2020.

[28] C. D. of Motor Vehicles, "Vehicle positioning," 2021. [Online]. Available: https://www.dmv.ca.gov/portal/es/handbook/california-driver-handbook/vehicle-positioning/

[29] W. B. Nicholson, D. S. Matteson, and J. Bien, "Varx-l: Structured regularization for large vector autoregressions with exogenous variables," *International Journal of Forecasting*, vol. 33, no. 3, pp. 627–651, 2017.

[30] L. Breiman and A. Cutler, "Random forests," *Machine learning*, vol. 45, no. 1, pp. 5–32, 1994.

[31] W. Zhan, L. Sun, D. Wang, H. Shi, A. Clausse, M. Naumann, J. Kummerle, H. Konigshof, C. Stiller, A. de La Fortelle *et al.*, "Interaction dataset: An international, adversarial and cooperative motion dataset in interactive driving scenarios with semantic maps," *arXiv preprint arXiv:1910.03088*, 2019.

[32] X. Liao, X. Zhao, Z. Wang, Z. Zhao, K. Han, R. Gupta, M. J. Barth, and G. Wu, "Driver digital twin for online prediction of personalized lane change behavior," *IEEE Internet of Things Journal*, 2023.

[33] X. Liao, S. Mehrotra, S. Ho, Y. Gorospe, X. Wu, and T. Mistu, "Driver profile modeling based on driving style, personality traits, and mood states," in *2022 IEEE 25th International Conference on Intelligent Transportation Systems (ITSC)*. IEEE, 2022, pp. 709–716.